A Measurement of Photon Production in Electron Avalanches in CF_4

A. Kaboth [c,*] J. Monroe [c] S. Ahlen [a] D. Dujmic [c] S. Henderson [c]
G. Kohse [c] R. Lanza [c] M. Lewandowska [a] A. Roccaro [a]
G. Sciolla [c] N. Skvorodnev [b] H. Tomita [a] R. Vanderspek [c]
H. Wellenstein [b] R. Yamamoto [c] P. Fisher [c]

[a] *Boston University, Boston, MA 02215*
[b] *Brandeis University, Waltham, MA 02454*
[c] *Massachusetts Institute of Technology, Cambridge, MA 02139*

Abstract

This paper presents a measurement of the ratio of photon to electron production and the scintillation spectrum in a popular gas for time projection chambers, carbon tetrafluoride (CF_4), over the range of 200 to 800 nm; the ratio is measured to be 0.34±0.04. This result is of particular importance for a new generation of dark matter time projection chambers with directional sensitivity which use CF4 as a fill gas.

Key words: Gas properties, Gas scintillation, Optical readout

1 Introduction

An interesting unsolved problem in physics is the nature of dark matter. Astronomical observations have shown that dark matter comprises approximately 22% of the energy in the universe [1], yet there is no strong evidence for direct detection of a dark matter particle. One of the most popular dark matter candidates is the lightest supersymmetric particle, the neutralino [2]. The motion of the solar system about the galactic center is expected to produce an apparent dark matter wind [3]. Directional dark matter experiments use gas-filled

* Corresponding author.
Email address: akaboth@mit.edu (A. Kaboth).

time projection chambers with electronic [4,5] or optical readout [6] to search for this wind. The signal is a directional asymmetry in dark matter induced nuclear recoils. Recoiling nuclei are detected via energy deposition in the gas, producing scintillation photons and ionization electrons.

A particularly appealing gas is carbon tetrafluoride, CF_4, because supersymmetric dark matter has an enhanced spin-dependent cross-section with fluorine [7]. CF_4 gas also has a number of experimentally desirable features: it has a high electron drift velocity, typically 10 cm/μs [8], and it emits a large number of scintillation photons in the UV and visible light regions of the spectrum [9], with a significant fraction of the photons falling in the visible region of the spectrum. This last feature is critical for experiments aiming to employ optical readout of detectors with CCD cameras [6].

This paper presents a measurement of the ratio of photons to electrons produced in CF_4 over the range 200-800 nm. Panksy, et al. [9] measured this ratio to be 0.3$\pm$0.15 in the wavelength range of 160-600 nm. Extending the range to 800 nm is interesting because many CCDs have high quantum efficiencies in the 600-800 nm range. This paper also presents the first wavelength dependent measurement of the scintillation spectrum of CF_4 between 200 and 800 nm.

2 Experimental Apparatus

A single wire proportional tube produces both electrons and photons from an electron-induced avalanche. The proportional tube is supplied with a Fe-55 source, which primarily produces K_α X-rays at 5.89 keV [10]. Since the work function of CF_4 is 54 eV [11], this results in approximately 110 primary electrons in the tube. These electrons are accelerated by a high electric field and collide with gas molecules, ionizing or exciting the target molecule in the collision. The electrons liberated by the ionization are in turn accelerated and ionize more molecules. This process creates an avalanche, which creates an electrical signal on the central axis wire, in conjunction with copious associated photons. Typical gains in this apparatus are of order 10^5.

The proportional chamber used for this measurement is a 6.5" long, 1" inner diameter copper tube with a 50 μm diameter copper wire in the center. The tube is operated at voltages on the central wire ranging from 2250-2425 V, with the tube walls at ground, which gives rise to electric fields ranging from 30-35 kV/m near the tube walls and 8100-8800 kV/m near the wire. The tube sits in a vacuum vessel with a 1" thick acrylic top. CF_4 gas is supplied to this vessel, such that the gas fills both in and around the proportional tube. Typical operating pressures range from 140-180 Torr at 24-27°C.

Table 1
Typical signal sizes through the data acquisition chain.

Portion of Electronics	Size(mV)	Duration or frequency (μs)
Wire	5-15	3-6 pulses every 0.105
PMT	50-200	3-6 pulses every 0.105
Wire preamplifier	50-300	5
PMT preamplifier (incl. 10x atten.)	15-75	50
Wire spectroscopic amplifier	500-2000	5
PMT spectroscopic amplifier	120-750	15
PMT with 1 photoelectron (p.e.)	30-50	20ns
PMT with 1 p.e. preamplifier (incl. 10x atten.)	1-2	50
PMT with 1 p.e. spectroscopic amplifier	6-10	15

The electron signal is collected from the central wire of the proportional tube. High voltage is supplied to the proportional tube through a 1000 kΩ resistor, and the signal is read out through a 1 nF blocking capacitor and a 1.5 kΩ resistor. The signal then is processed by an integrating preamplifier and an ORTEC model 672 spectroscopic amplifier. The output of the spectroscopic amplifier is fed into a LeCroy WaveSurfer 432 oscilloscope which acts as a trigger and analog-to-digital converter.

The photon signal is collected with a photomultiplier tube (PMT) placed on top of the acrylic vacuum vessel cover and centered over a 1" long and 1/16" wide slit, which is covered with a 1 mm thick quartz window, in the top of the proportional tube. The entire vacuum vessel and PMT combination is placed inside a dark box. The PMT used is a Hamamatsu H1161 [12]. The output of the PMT is fed into an ORTEC model 575A integrating preamplifier and a Canberra model 2005 spectroscopic amplifier and then into the oscilloscope.

Fig. 1(a) shows a sketch of the apparatus. Fig. 1(b) shows a schematic of the electronics chain. Table 1 shows typical signal sizes through the apparatus at a pressure of 180 Torr and 2375 V.

The purpose of this apparatus is to measure the photon to electron ratio in CF_4 in a generally applicable way. Thus, the efficiency and the acceptance of the apparatus is taken into account through a series of corrections described in the next section. These corrections include geometric acceptance, wavelength dependent transmission factors, PMT quantum efficiency, and the shape of the CF_4 photon emission spectrum.

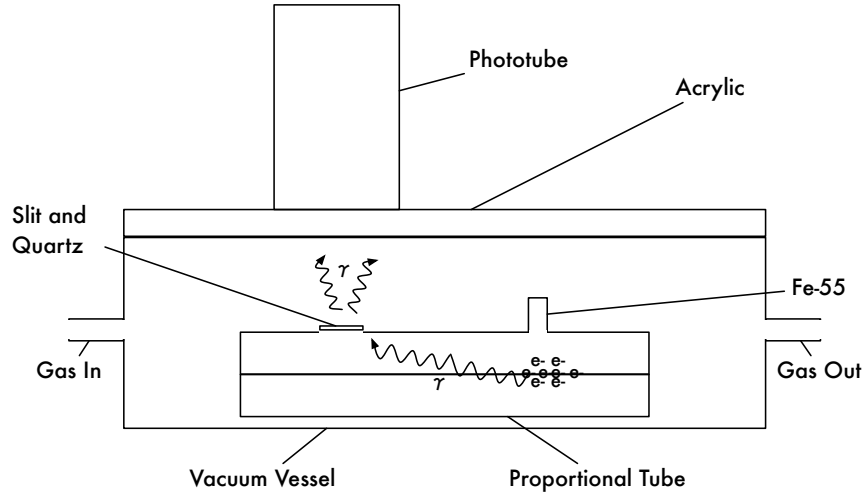

(a)

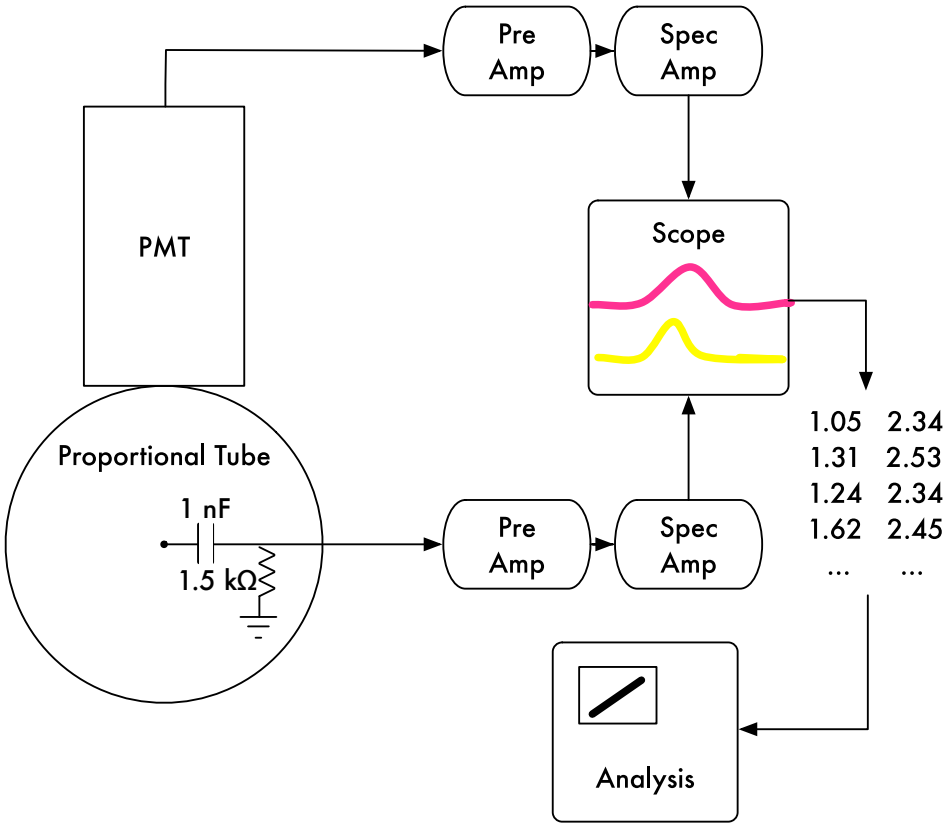

(b)

Fig. 1. (a): Side view, not to scale, of experimental apparatus. (b): Schematic of the electron and photon data acquisition chain.

3 Calibrations

3.1 Electron Signal

To measure the number of electrons in the avalanche, the amplitude of the wire signal spectroscopic amplifier pulses must be correlated to an absolute number of electrons. This is accomplished using a 10 pF test input on the integrating preamplifier. A known voltage placed across this capacitor translates into a known charge propagated through the electronics chain. A quadratic polynomial fits the calibration data best, corresponding to a small non-linearity in the preamplifier; a typical calibration is $N_{e^-} = (2.68\times\ 10^6)V_{sa}^2 + (4.50\times\ 10^7)V_{sa} + (4.62\times\ 10^6)$, where N_{e^-} is the number of electrons and V_{sa} is the spectroscopic amplifier output. Thus, a 4 V signal in the amplifier corresponds to 2.28×10^8 electrons.

3.2 PMT Signal

The number of photons is measured with a PMT, which is calibrated with a known light source. For this calibration, a green (565 nm) LED is placed in the apparatus next to the slit in the proportional chamber. The LED is pulsed with a narrow (100 ns) square wave at 1 kHz. The voltage of the square wave is adjusted until a single photon from the LED is detected by the PMT in about 10% of pulses, and zero photons the remainder of the time. Poisson statistics dictate that at this 10% occupancy, a two photon signal would be observed 0.5% of the time. This one photoelectron signal is fed through the PMT electronics chain and read out in the same way as a photon signal from an avalanche. The distribution of the number of events vs. PMT signal voltage is fit with two gaussians, corresponding to a pedestal and a signal peak. The mean of the signal peak corresponds to one photoelectron, and typically is 5 mV after pedestal subtraction. This calibration was repeated with 5% and 1% occupancy, and the results were consistent with the calibration at 10% occupancy. Thus, a 20 mV PMT signal corresponds to 4 photoelectrons.

3.3 Solid Angle Acceptance

The slit in the proportional tube only captures a small fraction of the isotropic light that is emitted in the avalanche at the approximate location of the interaction point of the Fe-55 X-rays. To measure this effect, the LED is attached to an optical fiber, which is placed in the opening for the Fe-55 source. The length of the fiber is adjusted so that the end of the fiber is as close to the

central wire as possible, since the bulk of the avalanche occurs within one wire radius of the wire's surface. The PMT is placed as shown in Fig. 1(a), and signals are read out through the entire electronics chain. Then the end of the fiber is affixed directly to the face of the PMT and again the signals are read out. The ratio of the mean PMT signal distribution from the fiber inside the tube to the fiber on the PMT gives a solid angle and transmission coefficient of 0.00073 ± 0.00012. The error on this number reflects the variation over several trials.

However, this value must be slightly corrected since the optical fiber is not isotropic, but rather directs most of the light in one direction. This correction is done using a simulation which bounces photons off of the reflective surface of a cylinder. The difference between light tightly focused in one direction and isotropic light gives rise to a correction of +5%. Dividing by the value of acrylic transmission at 565 nm (see Section 3.4) gives the value of the solid angle acceptance alone. No correction is made for the transmission of the quartz window, as the window had been removed when this measurement was made. Thus, the final value for the solid angle acceptance is 0.00083 ± 0.00017, where the error includes the measurement error, along with a 5% error related to the anisotropy and a small error from the transmission correction. A calculation of just the angle subtended by the slit gives a solid angle factor of 0.0002. This calculation is confirmed by setting the reflectivity of the simulation to zero.

3.4 Detector Transmission Functions

Light from the avalanche is attenuated by the quartz window and the acrylic vacuum vessel cover before reaching the PMT. The transmission of both materials is measured with a Jobin-Yvon 1250M spectrometer using an ultraviolet-sensitive Hamamatsu R928 multialkali PMT [13], with an incandescent lightbulb providing a continuous input spectrum.

The measured transmission curve of the acrylic is shown in Fig. 2.

The measured quartz transmission curve is shown in Fig. 3. This result is startling because the transmission is so low; the normal transmission of quartz is around 0.95 across all wavelengths of interest. This piece of quartz, however, had a crystalline growth on it, which accounts for the severely attenuated transmission. The level of growth was assumed to be constant over one month of data collection.

The PMT response is also wavelength dependent; Fig. 4 shows the quantum efficiency of the photomultiplier tube [12].

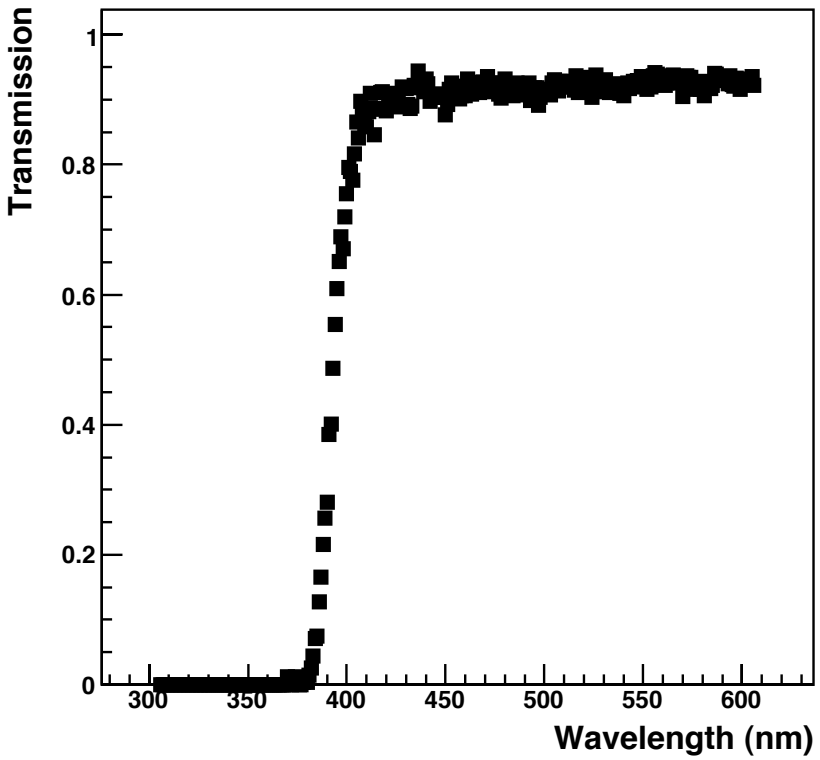

Fig. 2. Measured fractional transmission through acrylic, using an incandescent light source, versus wavelength in nm.

3.5 CF_4 Spectrum

To report the ratio of photons to electrons in an apparatus independent way, the observed number of photons must be corrected for the fraction of the total spectrum that is observable in this particular apparatus. Note that the spectrometer replaces the PMT in Fig 1(a); that is, the spectrum is measured through the same slit used in counting photons from the avalanche. Fig. 5 shows the measured emission spectrum. The spectrum is normalized to unit area, because the fraction of observable photons depends only on the shape of the spectrum, not its normalization. The spectrum was taken in 2 nm steps with the same spectrometer used in the transmission measurements. The spectrum has been corrected for second order diffraction at wavelengths above 400 nm; below 200 nm, oxygen in the air absorbs any photons, and so light from 200 to 400 nm has no second order component. The light intensity above 400 nm is given by the equation

$$I^{obs}(\lambda) = QE(\lambda) \cdot I^{true}(\lambda) + f \cdot QE(\frac{\lambda}{2}) \cdot I^{true}(\frac{\lambda}{2})$$

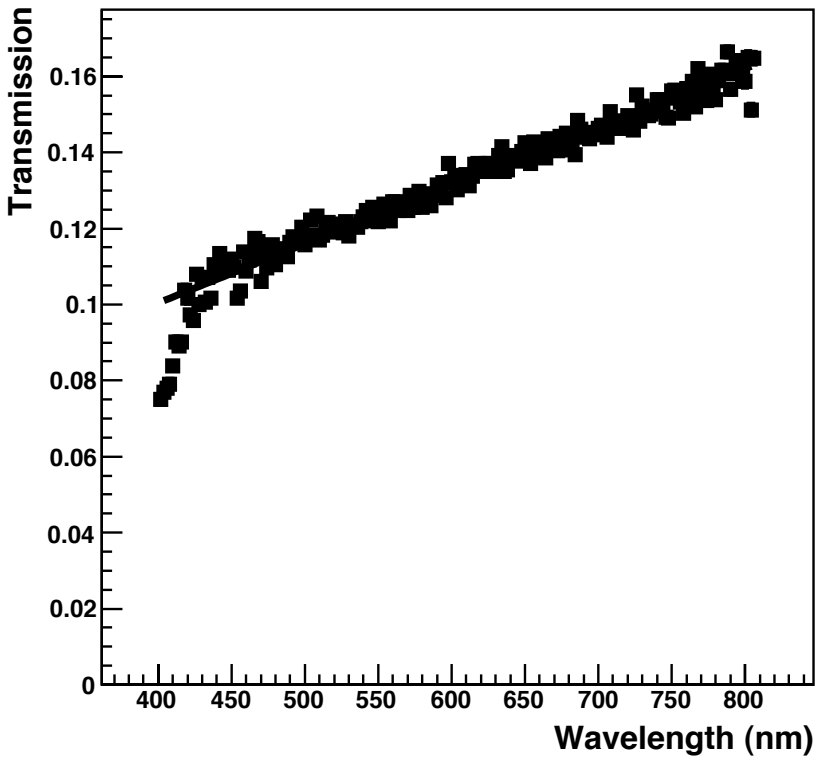

Fig. 3. Measured fractional transmission through quartz, using an incandescent light source, versus wavelength in nm.

, where f is the fraction of second order light, and $QE(\lambda)$ is the wavelength dependent quantum efficiency of the spectrometer phototube. Since the quantum efficiency is known, if f is known, then the above equation can be solved for $I^{true}(\lambda)$. The value of f can be measured by taking the spectrum of an ultraviolet source both in the UV and in the visible, with and without a filter with a cutoff near 400 nm, and then comparing the intensity in the visible to that in the UV, after correcting for the transmission of the filter. In this spectrometer, $f = 0.25 \pm 0.1$.

This is the first measurement of this spectrum between 200 and 800 nm. Note that 58% $\pm$ 6% of the spectrum is above 450 nm. This is particularly interesting, since the quantum efficiency of most CCDs turns on around 450 nm and peaks around 600 nm, indicating that CCD readout is well-matched to the CF_4 spectrum. See Ref. [14] for an explanation of the excitations of the CF_4 molecule that give rise to the 300 nm and 630 nm peaks. Note also a few transition lines in the spectrum; the origins of these lines are not described in the literature, and could be a point of further study.

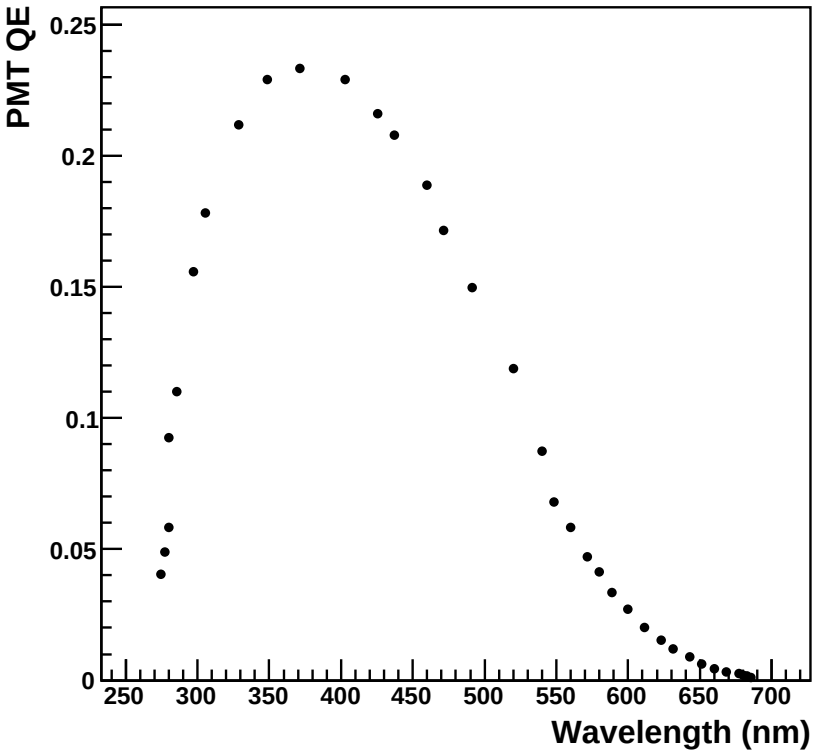

Fig. 4. PMT quantum efficiency versus wavelength in nm for the Hamamatsu H1161 PMT [12] used in the experimental apparatus.

The spectrum measured by the PMT in the proportional tube apparatus, shown in Fig. 6, is computed within each wavelength bin with the formula

$$I_{observed} = I_{spectrum} \cdot T_{acrylic} \cdot T_{quartz} \cdot QE_{PMT}$$

where $I_{spectrum}$ is the total CF_4 spectrum, $T_{acrylic}$ is the transmission through acrylic, T_{quartz} is the transmission through quartz, and QE_{PMT} the PMT quantum efficiency. By integrating this spectrum and comparing with the raw CF_4 spectrum, an overall wavelength dependent correction factor of 0.0035 ± 0.0002 is found. Figs. 5 and 6 do not show error bars, but the statistical error on the spectrum, as well as the errors contributed from background subtraction and multiplying by the quartz and acrylic transmission curves are included in finding the correction factor error. Typical relative errors on the raw spectrum are 30% and on the convoluted spectrum are 50%. Because the integral is performed as a sum, the relative error on the final correction factor is significantly reduced, because of the properties of propagation of errors in addition. Table 2 shows the relative size of the corrections to the photon measurement. Combining all of these corrections gives

$$N_{\gamma}^{measured} = C_{sa} \cdot C_{\lambda} \cdot N_{\gamma}^{true}$$

where C_λ is the wavelength dependent correction factor, C_{sa} is the solid angle correction factor.

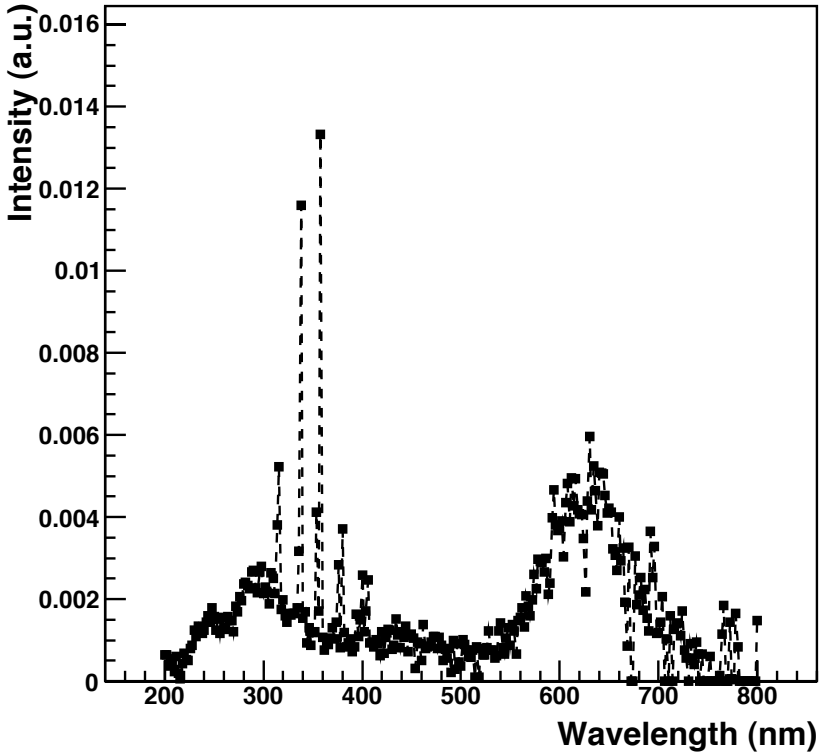

Fig. 5. Measured CF_4 scintillation spectrum in arbitrary units of intensity versus wavelength in nm. The integral is normalized to unity. For clarity, error bars are not shown. The spectrum is corrected for the spectrometer PMT quantum efficiency.

4 Results

4.1 Voltage and Pressure Dependancies

The number of electrons and photons in the avalanche were measured for a range of pressures and wire voltages. Fig. 7(a) shows the number of electrons (solid circles) and photons (open circles) produced in the avalanche as a function of voltage at 180 Torr; Fig. 7(b) shows the same as a function of pressure for 2325 V. Comparing the two processes, it is clear that the photon emission and the electrons production are linked, as they show similar functional dependance on the two variables of wire voltage and pressure.

The interpretation of the data, beyond the general trend that the avalanche

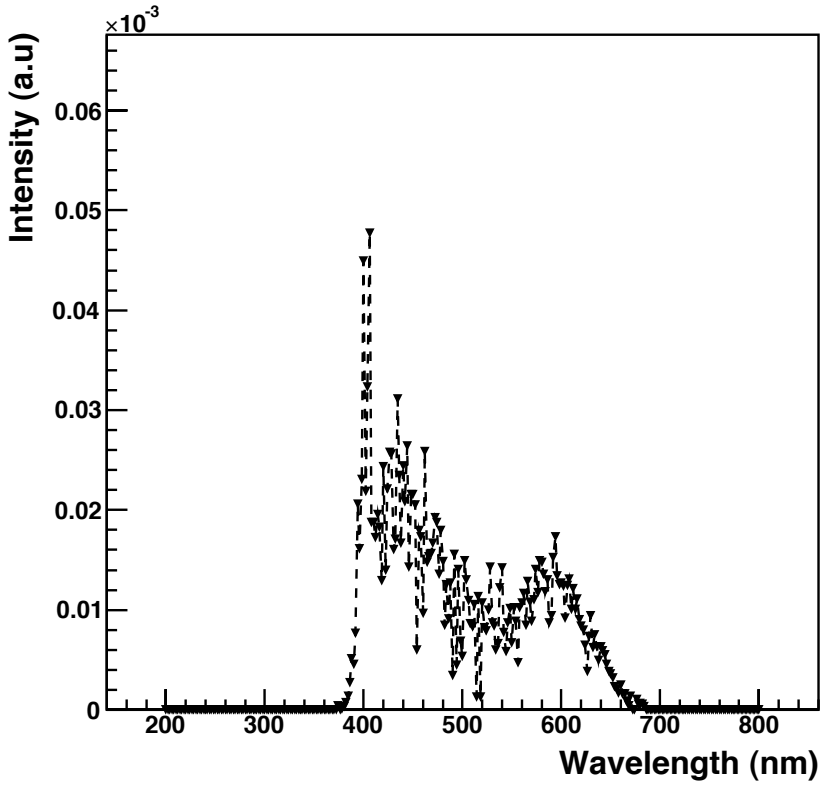

Fig. 6. Observed photon spectrum at the apparatus PMT in arbitrary units of intensity versus wavelength in nm. The scale of the intensity is the same as in Fig. 5. For clarity, error bars are not shown. Each bin is the product of the true CF_4 spectrum, the acrylic and quartz transmittance, and the PMT quantum efficiency.

Table 2
Corrections to PMT measurements. Note that while the total wavelength dependent correction is dependent on the PMT quantum efficiency, as well as the quartz and lucite transmission, it is not the direct product of the three individually integrated over the whole spectrum, but rather the product of the three in each wavelength bin, then integrated over the whole spectrum.

Correction	Value	Relative Error
PMT Calibration	1	0.04
Solid Angle	0.00083	0.20
Total Wavelength Dependent	0.0035	0.0002
PMT Quantum Efficiency	0.064	0.002
Lucite Transmission	0.71	0.04
Quartz Transmission	0.124	0.007

multiplication increases sharply with voltage and decreases sharply with pressure, is difficult. CF_4 scintillates in ultraviolet, and the UV photons striking the side of the proportional tube eject electrons, which create secondary avalanches; as a result one Fe-55 decay can produce up to 10 avalanches. Since the number of avalanches is not constant for a given wire voltage, this makes it difficult to calculate the gain, $N_{e^-}^{avalanche}/N_{e^-}^{primary}$. An interesting side-effect of this phenomenon is an easy way to estimate the drift velocity in CF_4. Since the pulses come an average of 105 ns apart, and the radius of the tube is half an inch, the corresponding drift velocity is approximately 12 cm/μs. This is in good agreement with [15], at the field near the edge of the tube, 35 kV/m, at 180 Torr (1.48 kV/cm/atm).

4.2 N_γ/N_{e^-}

While the gain of the gas is expected to vary with pressure and voltage, the ratio of photons to electrons should be invariant, as it is an intrinsic property of the gas. The data validates this hypothesis, and therefore all of the data can be combined to calculate the ratio. Fig. 8 shows the number of photons as a function of the number of electrons for all data after all calibrations and corrections have been applied. A first-degree polynomial describes the data well; this is the functional form used to fit the data. The fitted line is also constrained to pass through the origin, corresponding to a detector limit of zero photons emitted when zero electrons are present. The slope of this line, 0.34 ± 0.04, gives the number of photons emitted per electron in the avalanche. This ratio is measured over the range of 140-180 Torr and 2150-2425 V.

4.3 Discussion

The largest source of uncertainty in this measurement comes from the variations of experimental conditions between runs. This variation can come from a number of factors, the most prominent of which are variations in gas pressure and contamination. The measured leak rate of the vacuum vessel is $5\text{x}10^{-6}$ Torr/L·s, with the result that taking data over the span of four hours leads to contamination of 0.2% of the CF_4 with air. Furthermore, different levels of contamination before filling the vessel with CF_4 can affect the run to run performance. Local temperature and humidity variations can also affect the level and nature of contamination, as well as the performance of the PMT.

The error resulting from the variation between runs is taken into account in the error bars of Fig. 8. A scatterplot of N_γ vs. N_{e^-} is made from all the data. Then a profile plot is created using the spread of the data points in each bin of the histogram when calculating the errors, instead of the root mean square

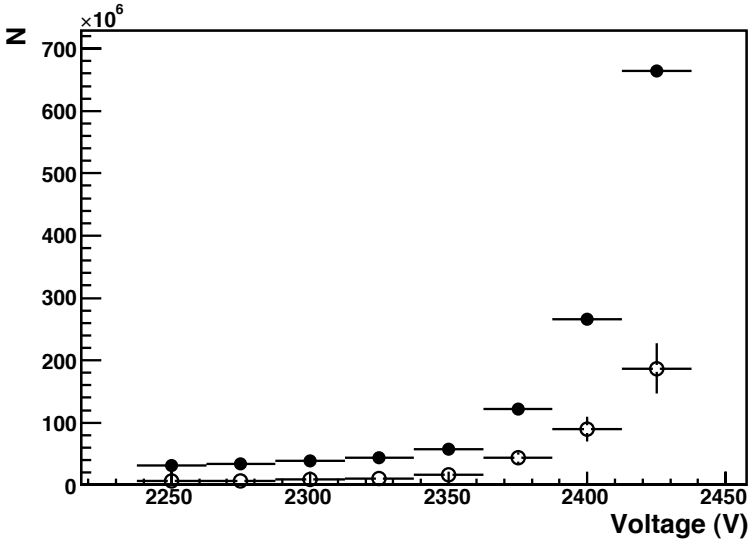

(a)

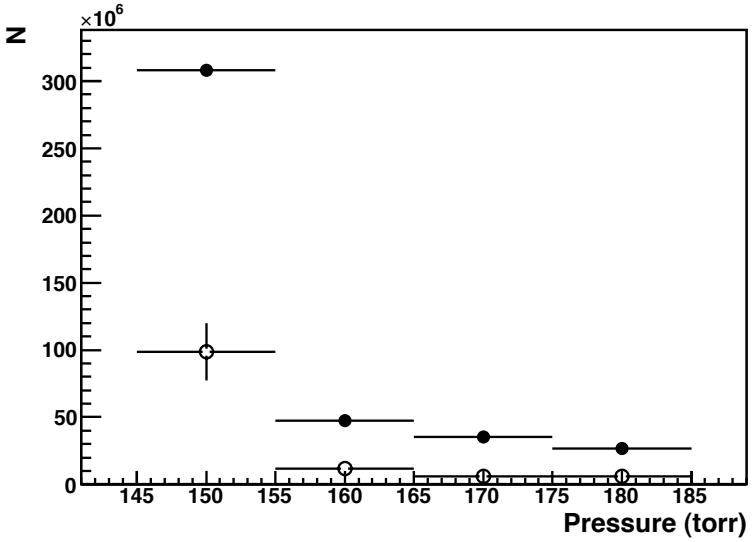

(b)

Fig. 7. Pressure and voltage dependence of photon and electron production. Open circles show photons, filled circles show electrons. (a): Number of electrons and photons versus voltage at 180 Torr CF_4 pressure. (b): Number of electrons and photons versus pressure at 2325 V wire voltage.

(RMS). The reason for this choice is that in each bin of number of electrons, several data sets are combined. If only one data set were used to make this plot, the projection of this bin onto the y-axis (number of photons) would be gaussian, and the error on the mean would be the appropriate error. However, since the projection is, in fact, non-gaussian, the spread better describes the error on the mean. Typical errors are 50%. The errors introduced from the solid angle and wavelength-dependent factors are then also included in the

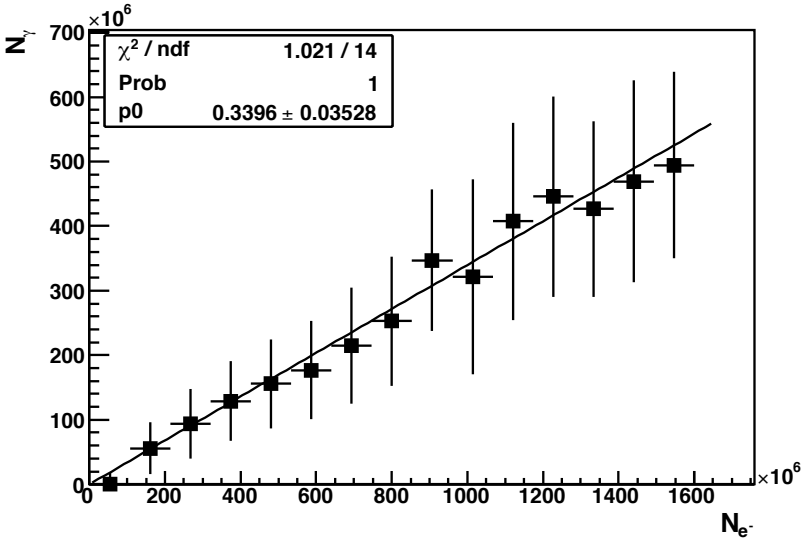

Fig. 8. Number of photons vs number of electrons, fit with a line passing through zero. The data are a combination of several data sets of varying pressure and voltage. The slope of the fit line, 0.34 ± 0.04, is the ratio of photons to electrons produced in avalanches in CF_4.

error bars of Fig. 8, added in quadrature with the error from the spread. Note that the correct choice of error when making the plot has a significant effect on the error of the fit; using the spread instead of the RMS increases the error on the photon to electron ratio by approximately a factor of two.

The measured ratio of photons to electrons, 0.34 ± 0.04 is in agreement with the Pansky et. al. measurement of 0.3 ± 0.15 [9], but improves on the relative error by a factor of five. Furthermore, the Pansky measurement was made at 10 Torr, and this measurement was made at 140-180 Torr, which is more typical of current and proposed experiments using CF_4 as a detection technique for dark matter.

5 Conclusions

This paper presents measurements of two critical properties of CF_4 gas: the ratio of photons to electrons produced in an avalanche, 0.34 ± 0.04, and the scintillation spectrum between 200 and 800 nm, shown in Fig. 5 with 10% bin-to-bin errors, with the interesting observation that CCD quantum efficiency and the CF_4 spectrum are well-matched. With a firm grasp of these important properties, the prospects for optical readout of dark matter detectors using CF_4 as a target are good.

6 Acknowledgments

The authors would like to thank Ulrich Becker, Scott Sewell, and the MIT Junior Laboratory for their assistance. This work is supported by the Department of Defense National Defense Science and Engineering Graduate Fellowship, the Pappalardo Fellowship, and the Department of Energy Advanced Detector Research Program.

References

[1] D. Spergel, et al., Astrophys. J. Suppl 148 (2003) 175.

[2] J. Ellis, K. Olive, Y. Santoso, V. Spanos, Phys. Rev. D 71 (9) (2005) 95007.

[3] A. Drukier, K. Freese, D. Spergel, Phys. Rev. D 33 (12) (1986) 3495–3508.

[4] G. Alner, et al., Nucl. Instrum. Meth. A 555 (1-2) (2005) 173–183.

[5] K. Miuchi, et al., Phys. Lett. B 654 (3-4) (2007) 58–64.

[6] D. Dujmic, et al., Nucl. Instrum. Meth. A 584 (2) (2008) 327–333.

[7] D. Tovey, et al., Phys. Lett. B 488 (1) (2000) 17–26.

[8] J. Va'Vra, Nucl. Instrum. Meth. A 323 (1-2) (1992) 34–47.

[9] A. Pansky, et al., Nucl. Instrum. Meth. A 354 (2) (1995) 262–269.

[10] D. Lide, et al., Handbook of Chemistry and Physics, CRC Press Boca Raton, FL, 1995.

[11] A. Sharma, SLAC-Journal-ICFA 16 (1998) 3.

[12] Hamamatsu Photonics, Hamamatsu Phototube H1161, obtained in private communication with Hamamatsu.

[13] Hamamatsu Photonics, Hamamatsu Phototube R928, http://sales.hamamatsu.com/assets/pdf/parts_R/R928.pdf.

[14] M. Fraga, et al., Nucl. Instrum. Meth. A 504 (1-3) (2003) 88–92.

[15] J. Va'Vra, P. Coyle, J. Kadyk, J. Wise, Nucl. Instrum. Meth. A 324 (1-2) (1993) 113–126.

A Table of Values for CF_4 Spectrum

Note that where the intensity given is 0, this is due to background subtraction (the fluctuation dominates in that bin), but in all cases where the intensity is "negative", the value is consistent with zero.

Table A.1
CF_4 spectrum intensity, from 200-348 nm, unnormalized.

λ (nm)	I (a.u.)	ΔI (a.u.)	λ (nm)	I (a.u.)	ΔI (a.u.)	λ (nm)	I (a.u.)	ΔI (a.u.)
200	65.3145	83.1793	250	159.993	52.9829	300	217.379	56.7517
202	64.9513	77.1907	252	126.838	51.6025	302	233.081	57.3984
204	37.7948	70.909	254	154.446	52.5492	304	217.642	56.9136
206	54.3224	67.1186	256	119.075	51.0791	306	190.076	55.9737
208	40.0184	62.5843	258	156.888	52.4203	308	267.131	58.8478
210	23.9843	58.6422	260	134.347	51.4503	310	252.926	58.4195
212	61.476	58.664	262	128.501	51.1157	312	216.498	57.1792
214	20.384	55.4873	264	159.68	52.3001	314	384.908	63.1203
216	5.66265	53.4733	266	149.039	52.0261	316	528.661	67.8059
218	43.0572	53.7333	268	148.662	52.1418	318	176.739	55.9375
220	68.6155	53.5294	270	122.797	51.2778	320	200.179	56.8896
222	52.9467	51.6911	272	185.443	53.7872	322	160.849	55.4929
224	50.8944	50.4654	274	171.15	53.3864	324	146.318	55.016
226	80.9932	51.2871	276	208.986	54.9209	326	166.361	55.8361
228	88.2004	51.4579	278	199.511	54.7078	328	163.823	55.74
230	125.335	52.8039	280	239.663	56.3021	330	166.361	55.8361
232	110.288	52.0986	282	244.4	56.6083	332	167.207	55.8682
234	136.568	53.0044	284	236.57	56.4647	334	180.317	56.3622
236	119.53	52.2277	286	229.103	56.3333	336	321.574	61.4338
238	117.207	52.0215	288	269.804	57.9256	338	1175.04	85.9279
240	126.249	52.2585	290	273.044	58.1799	340	155.365	55.4181
242	144.956	52.8646	292	230.276	56.7941	342	170.59	55.9961
244	161.15	53.3663	294	218.17	56.4953	344	94.8868	53.0603
246	145.063	52.641	296	270.431	58.5051	346	132.104	54.5233
248	180.456	53.8639	298	283.269	59.0329	348	88.12	52.7899

Table A.2
CF_4 spectrum intensity, from 350-498 nm, unnormalized.

λ (nm)	I (a.u.)	ΔI (a.u.)	λ (nm)	I (a.u.)	ΔI (a.u.)	λ (nm)	I (a.u.)	ΔI (a.u.)
350	120.262	54.0621	400	261.469	64.734	450	116.828	71.0576
352	121.954	54.1282	402	121.493	59.7523	452	106.724	71.2801
354	417.578	64.6539	404	173.932	61.8298	454	31.1921	69.6012
356	173.974	56.1237	406	249.323	64.9429	456	95.7981	73.3892
358	1349.7	90.1239	408	93.9101	59.6254	458	92.9047	73.4476
360	108.202	53.6816	410	96.5054	59.9044	460	51.6535	72.056
362	76.9956	52.5315	412	83.8492	59.6386	462	140.349	76.5034
364	92.0338	53.2321	414	102.526	60.6747	464	81.0909	75.5488
366	91.3611	53.302	416	91.7378	60.5796	466	85.2531	75.8922
368	106.486	54.0005	418	62.9991	60.2199	468	87.1913	76.1723
370	131.94	55.0955	420	123.008	63.3731	470	95.8144	77.0681
372	103.904	54.0939	422	69.5993	61.3572	472	111.003	78.2183
374	145.346	55.8105	424	108.868	62.9983	474	110.272	79.0595
376	287.237	61.1277	426	128.814	64.119	476	80.4428	78.8334
378	82.9566	53.5532	428	125.327	64.3539	478	108.772	81.0608
380	375.662	64.3694	430	79.1971	63.3466	480	88.0652	81.5078
382	119.256	55.2093	432	87.634	64.5492	482	51.5956	81.339
384	84.5598	54.0615	434	153.941	67.8935	484	78.4339	83.5651
386	95.4375	54.73	436	113.924	67.2079	486	56.1069	82.9831
388	104.22	55.3144	438	82.3555	66.2183	488	80.3494	84.1533
390	72.0601	54.2596	440	121.29	67.9524	490	21.5875	83.8431
392	84.3609	54.9963	442	107.651	67.8507	492	99.5699	88.7153
394	164.453	58.3762	444	136.337	69.3701	494	29.1645	86.2423
396	109.309	56.4777	446	73.7305	67.856	496	92.6976	88.7257
398	151.173	58.3587	448	111.892	70.2786	498	46.4752	86.7559

Table A.3
CF_4 spectrum intensity, from 500-648 nm, unnormalized.

λ (nm)	I (a.u.)	ΔI (a.u.)	λ (nm)	I (a.u.)	ΔI (a.u.)	λ (nm)	I (a.u.)	ΔI (a.u.)
500	36.4849	86.1801	550	89.2489	114.22	600	375.581	160.983
502	102.641	90.3827	552	140.487	116.652	602	396.298	162.189
504	89.6291	91.6857	554	123.371	119.097	604	307.501	159.743
506	76.185	90.9067	556	66.41	120.347	606	441.883	164.152
508	61.0873	90.1295	558	150.069	124.65	608	487.941	165.661
510	59.6232	92.1965	560	156.539	126.316	610	394.243	168.623
512	76.4439	95.0953	562	180.365	127.912	612	502.845	178.548
514	9.59214	92.437	564	134.692	127.205	614	432.149	176.636
516	83.9446	95.1063	566	211.043	130.74	616	499.523	179.178
518	9.5425	92.7015	568	184.317	130.785	618	422.519	175.592
520	81.109	95.8827	570	161.737	133.686	620	413.263	174.281
522	64.99	97.0012	572	200.037	138.831	622	411.966	187.527
524	65.5319	98.8485	574	263.806	142.617	624	352.283	201.435
526	81.8819	99.7023	576	228.699	143.209	626	220.057	213.013
528	124.516	101.538	578	300.985	144.578	628	445.513	235.716
530	77.605	100.46	580	295.266	143.512	630	603.457	208.065
532	76.8365	101.096	582	293.906	144.389	632	422.403	178.175
534	56.2859	100.054	584	269.862	144.528	634	532.268	184.801
536	63.7774	100.12	586	303.549	150.368	636	469.454	185.658
538	123.261	105.324	588	215.322	152.109	638	384.704	181.83
540	144.125	109.465	590	242.004	155.174	640	514.759	185.582
542	83.1506	107.608	592	403.651	162.596	642	513.66	186.306
544	66.2024	107.339	594	472.805	162.011	644	511.235	187.021
546	105.547	111.419	596	386.357	156.666	646	458.367	187.92
548	131.109	115.109	598	371.513	158.476	648	415.111	189.259

Table A.4
CF_4 spectrum intensity, from 650-798 nm, unnormalized.

λ (nm)	I (a.u.)	ΔI (a.u.)	λ (nm)	I (a.u.)	ΔI (a.u.)	λ (nm)	I (a.u.)	ΔI (a.u.)
650	426.926	191.24	700	120.682	225.586	750	0	293.755
652	417.266	192.497	702	146.175	256.884	752	60.5802	287.798
654	327.236	191.243	704	207.998	300.511	754	0	316.024
656	311.523	192.665	706	0	262.753	756	0	362.564
658	273.808	193.221	708	105.268	244.81	758	0	324.491
660	406.299	199.916	710	0	413.9	760	0	304.701
662	297.686	198.718	712	161.009	663.26	762	14.0033	310.697
664	329.468	202.539	714	0	403.65	764	115.306	316.502
666	194.843	210.949	716	127.787	242.856	766	186.199	325.06
668	86.9937	223.037	718	140.813	243.233	768	0	318.339
670	330.508	342.312	720	144.438	243.434	770	0	324.114
672	0	473.582	722	111.954	245.155	772	145.036	341.582
674	0	312.183	724	172.941	250.655	774	6.19413	338.65
676	309.099	209.622	726	76.1387	248.95	776	4.21727	341.51
678	189.65	208.318	728	57.3759	250.348	778	167.01	354.912
680	212.602	212.348	730	0	250.834	780	85.5268	358.783
682	256.281	210.695	732	93.4533	258.485	782	0	367.785
684	175.286	205.101	734	56.6552	261.381	784	0	380.855
686	225.424	211.389	736	42.0142	265.915	786	0	380.178
688	156.446	213.468	738	95.5614	268.966	788	0	382.555
690	123.705	211.65	740	67.5604	269.02	790	0	398.214
692	369.487	220.837	742	0	273.198	792	0	405.17
694	255.217	220.764	744	67.177	283.406	794	0	417.16
696	332.219	228.197	746	0	298.388	796	0	450.477
698	118.388	222.757	748	0	310.516	798	0	445.163